PAPER

Check for updates

Hysteresis in the transfer characteristics of MoS$_2$ field effect transistors: gas, temperature and photo-irradiation effect†

Muhammad Shamim Al Mamun, [iD] *[ad] Yasuyuki Sainoo,[b] Tsuyoshi Takaoka, [iD] [b] Atsushi Ando[c] and Tadahiro Komeda [iD] [b]

We report the characteristic behaviors of the hysteresis observed in the transfer characteristics of back-gated field-effect transistors with an exfoliated MoS$_2$ channel under various conditions. We find that the hysteresis is strongly enhanced by temperature, environmental gas, or light irradiation. Our measurements reveal the characteristic hysteresis behaviors in a 1 atm oxygen environment, which we explain as an oxygen molecule facilitated charge acceptor on the MoS$_2$ surface. The decrease in the current value in the ON state of the device may indicate that oxygen molecules are more effective charge acceptors than nitrogen molecules. We conclude that intrinsic defects in MoS$_2$, such as S vacancies, which result in effective adsorbate trapping, play an important role in the hysteresis behavior, in addition to oxygen and nitrogen adsorbates on the passivated device surface. The availability of thermally or photo-generated minority carriers (holes) in MoS$_2$ is increased by both light and temperature. This leads to subsequent processes of positive charge trapping, which intensify the hysteresis.

Introduction

Molybdenum disulfide (MoS$_2$) has received much attention as the most popular semiconductor from the family of transition metal dichalcogenides.[1] The bulk form of MoS$_2$ is composed of stacks of two-dimensional layers that are weakly constrained by van der Waals interactions. Each MoS$_2$ layer is formed by three atomic planes, with the Mo plane sandwiched between two S planes. Since the interlayer bonds are weak, it is possible to obtain monolayer MoS$_2$ using scotch tape or liquid phase exfoliation, similarly to graphene.[2–5] Chemical vapor deposition (CVD) from heated S and MoO$_3$ powders has become the standard fabrication method for large-scale production.[6] Bulk MoS$_2$ has an indirect band gap of 1.2 eV, while monolayer MoS$_2$ has a direct band gap of 1.8 eV.[7,8] This large bandgap, combined with mechanical flexibility, makes MoS$_2$ suitable as a channel for field-effect transistors (FETs) for logic applications.

Hysteresis features appear as two well-separated current levels, especially when gases are stably adsorbed on the channel, and can be exploited in memory devices. Chalcogen vacancies favor natural n-type doping in MoS$_2$ and act as trap centers that enhance the hysteretic behavior in MoS$_2$ and other 2D TMDs.[9–11]

Initial studies of the photo-response of TMD films were carried out at room temperature and in air. At this stage, no claims were made about the decay time of the photocurrent. The rise and decay in the time-resolved photocurrent after switching on and off 532 nm laser illumination under various conditions revealed that adsorbent impurities are an important player in determining the time decay of photocurrents after irradiation with light.[12] Furthermore, even if a pure (pristine) MoS$_2$ surface was prepared, time decay of the photocurrent was observed. More recently, researchers have focused on the trap states caused by defects or residual impurities at MoS$_2$/SiO$_2$ interfaces. However, the effect of environmental gas conditions, temperature and light irradiation on the photo-response of MoS$_2$ devices is still unclear.

In this paper, we fabricate back-gated, exfoliated-MoS$_2$ transistors and investigate the effects of environmental conditions, temperatures and light irradiation on the hysteresis behavior. Our study confirms that hysteresis is enhanced by oxygen molecules adsorbed on the device surface and can be quenched by reducing the pressure or the temperature. Our experimental findings suggest that hysteresis is strongly related to oxygen adsorption on the gate channel, which facilitates charge transfer and trapping, and is favored when thermally generated or photogenerated minority carriers (holes) become available in the n-type MoS$_2$ transistor. We suggest that intrinsic

[a]Department of Chemistry, Graduate School of Science, Tohoku University, Aramaki-Aza-Aoba, Aoba-Ku, Sendai 9808578, Japan. E-mail: s.mamun@chem.ku.ac.bd

[b]Institute of Multidisciplinary Research for Advanced Materials (IMRAM, Tagen), Tohoku University, 2-1-1, Katahira, Aoba-Ku, Sendai 9800877, Japan

[c]National Institute of Advanced Industrial Science and Technology, 1-1-1 Umezono, Tsukuba, Ibaraki 305-8568, Japan

[d]Chemistry Discipline, Khulna University, Khulna, 9208, Bangladesh

defects such as S vacancies or other interfacial states, which result in effective positive charge trapping, are an important cause of hysteresis.

Experimental

We started by ultrasonicating a wafer (300 nm SiO_2 on $p^{++}Si$ substrate) in the solvents acetone and isopropanol for five minutes each. A thicker SiO_2 layer may lower the leakage currents and hysteresis, but can also have an impact on the overall device performance by slowing the switching speed and raising series resistance. On the other hand, while thinner SiO_2 layers provide greater electrostatic control, they are more vulnerable to leakage problems and hysteresis.[13] Thus, optimization of the dielectric thickness is important. In our previous studies, 300 nm SiO_2 was used successfully.[14–16] The substrate was further cleaned using a 30 min UV-O_3 treatment after being dried using a N_2 gas flow. The MoS_2 flake was transferred to SiO_2 on a Si substrate using the mechanical exfoliation technique with scotch tape.[17–19] In short, a piece of 3 cm scotch tape was cut, and a small amount of bulk MoS_2 was placed on the tape. Next, using two hands, the scotch tape was twisted so that the separated MoS_2 flakes covered nearly the entire surface of the scotch tape. Then, the MoS_2 flakes were placed on the $p++Si$ substrate by simply flipping the scotch tape. The thickness of the MoS_2 layer was estimated (i) by measuring the contrast of the reflected light from the SiO_2 surface with and without the MoS_2 flakes,[20] (ii) using Raman spectroscopy[21] and (iii) using atomic force microscopy (AFM).[22] The contrast was defined using the following equation:

$$C(\lambda) = \frac{R_0(\lambda) - R(\lambda)}{R_0(\lambda)}$$

where $R_0(\lambda)$ and $R(\lambda)$ are the intensities of the reflected light without and with MoS_2 for the wavelength λ, respectively. It has been suggested that the use of λ in the red region is more efficient compared to the use of blue and green lights.[3]

MMA (methyl methacrylate) and PMMA (poly(methyl methacrylate)) resists were applied on the flake. Electrode patterning was conducted using electron beam lithography (ELS-700, ELIONIX). Following development, an electron-beam evaporator was used to form the source and drain contacts of Ti (10 nm)/Au (150 nm). Ultimately, N-methyl-2-pyrrolidone (NMP) was used in a wet removal procedure to carry out the lift-off operation. A wire bonding machine (7476D, WEST-BOND) was used to wire the produced device on a Cu-epoxy circuit board using Al wire (0.05 mm, 1% Si/Al). The MoS_2-FET device's FET characteristics were assessed using an external source measure unit (SMU 2634, Keithley), to which SMA cables were used to link both the device and the electric feedthrough that was connected to the UHV chamber. Two rotary pumps and one ion pump were used to maintain a high vacuum of 10^{-6} Pa. External gas cylinders were used to pass the oxygen and nitrogen gas into the chamber. A depiction of the UHV chamber and gas transfer process is shown in Fig. S2.†

The electrodes for the source and the drain were formed by depositing Ti layers followed by Au layers. The device was mounted under a continuous flow cryostat LT3B Helitran® (ADVANCED RESEARCH SYSTEMS) in the vacuum chamber. Two LED arrays faced to the device surface were mounted on the linear motion feedthrough as displayed in Fig. 1 (a) side view and (b) angle view, which were attached inside the vacuum chamber and used as the light sources, as shown in Fig. 1 (c) for UV light and (d) for green light. The distance between the LED and MoS_2 device was set to around 5 mm. The wavelengths of the LEDs were 365 and 525 nm. The transfer and output characteristics of the devices were measured using a Keithley 2634B source measure unit. The signal coaxial cables were connected via electrical feedthrough to the measurement system.

Results and discussion

Fig. 2(a) shows an optical image of the back-gated FET device with four layers of MoS_2 flakes. The channel length and width of the sample are $L = 3.0$ μm and $W = 3.9$ μm, respectively. The $C(\lambda)$ of the red light was found to be 0.58, which indicated the number of the layers of the flakes to be four.[3] The Raman spectrum of the MoS_2 flakes was also obtained to determine the flake thickness, and is displayed in Fig. 2(b). The separation of 24.4 cm^{-1} between the two characteristic peaks (A_{1g} and E_{2g}) indicated four-layer MoS_2 flakes. AFM also confirmed that the MoS_2 flake thickness is about four layers (2.9 nm), as shown in Fig. S3.† Fig. 2(c) shows the transfer characteristics (I_{ds}–V_g curves, where I_{ds} is the drain-source current and V_g is the gate voltage) under ambient air, high vacuum (HV; 10^{-5} Pa) and ultra-high vacuum (UHV; 10^{-6} Pa). The HV condition was achieved by simple evacuation of air using a turbo-molecular pump for several hours, and UHV was achieved by baking the vacuum chamber (device temperature kept at ∼330 K) for 46 h followed by cooldown to room temperature for 14 h. We note that the on-state current at $V_G = 80$ V was increased by heating the device. The device exhibits n-type behavior, similar to previous reports.[23–26]

With lowering the pressure, the hysteresis was suppressed effectively. The decrement in the hysteresis with lowering the pressure indicates that the hysteresis is mainly attributed to the adsorbed molecules in air that act as charge-trapping centers. The transfer curves in different V_g sweep directions would be considerably affected by the trapped charges due to adsorbates on the device channel. This indicates that the hole (electron) trap is responsible for the negative (positive) shift of the transfer curve in the forward (backward) sweep direction, and the time constant for charge trapping/de-trapping is comparable to the measurement time with 5 V s^{-1} as shown in the present study. These results are highly consistent with various previous reports.[27–32]

After the device heating, on-state current at $V_G = 80$ V was improved ∼15%. Although residual gas, especially H_2O, should be removed, a small hysteresis still remained. This result indicates an intrinsic origin of hysteresis in the MoS_2 device, which was attributed to the presence of defects and point vacancies in the MoS_2 or charge traps at the interface.[33]

The intrinsic charge trapping effect in MoS_2 has a strong temperature dependance and should be suppressed by cooling
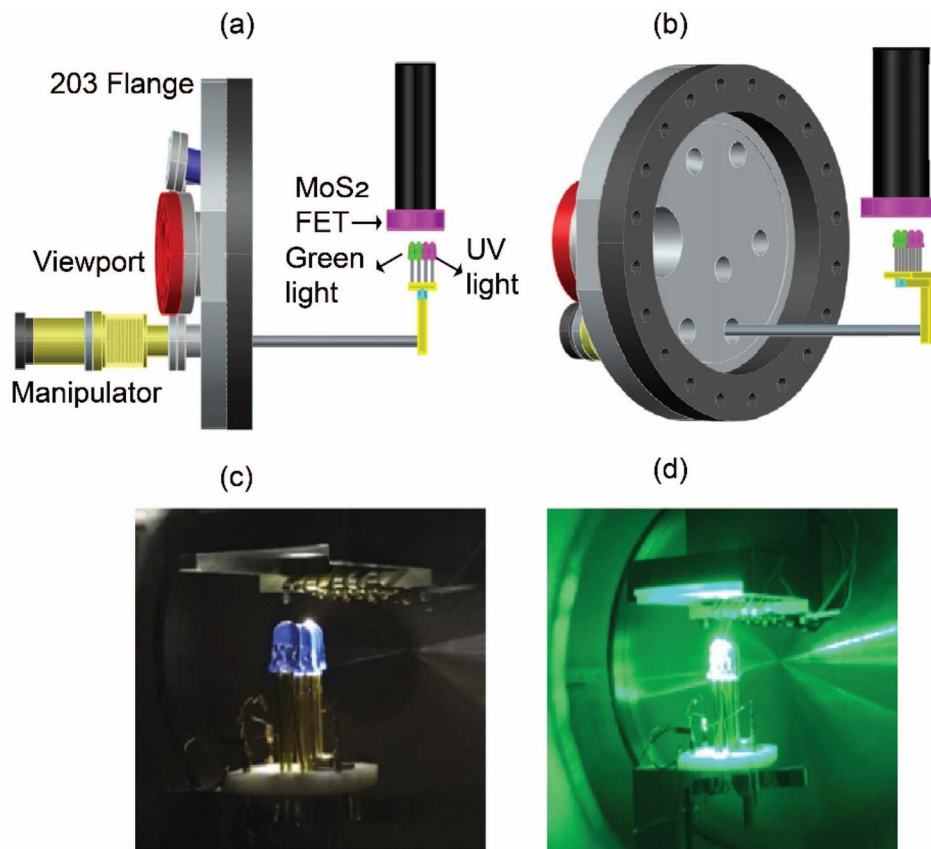
Fig. 1 Illustration of UV and green light irradiation system inside the *in situ* chamber: (a) side view, (b) angle view, (c) UV light irradiation of the MoS$_2$-FET, and (d) green light irradiation of the MoS$_2$-FET.

down the device. We observed a temperature effect in the hysteresis, as shown in Fig. 3. The hysteresis was drastically reduced when the device was cooled below room temperature to around 85 K, as shown in Fig. 3(a). Furthermore, the linearity of the transfer characteristics was improved at low temperature. These results indicate that the hysteresis ascribed to the charge trapping was almost suppressed at 85 K. The device was heated to around 370 K at 10^{-5} Pa overnight to ensure the removal of H$_2$O and impurities. After baking, we measured the transfer characteristics during the cooldown to room temperature, as shown in Fig. 3(b). While wider hysteresis was observed at higher temperature, the hysteresis decrease depended on the temperature during cooldown. A similar temperature dependence was observed for the other devices we fabricated. The disappearance of the hysteresis at low temperatures is attributed to the prolonged time constant for charge trapping/detrapping.[12,27] Thus, cooling the device in an easily attainable temperature range is one way to suppress the hysteresis or instability without surface passivation, which could be highly advantageous for the device applications of this system.

It is well known that water molecules strongly influence the magnitude of the hysteresis under ambient conditions.[34] We focused on the main components of the atmosphere other than water, namely, oxygen and nitrogen molecules, and studied the characteristics that appeared in the hysteresis. The device was heated to around 100 °C at 10^{-5} Pa overnight in both cases to ensure the removal of H$_2$O and impurities in the same manner as for Fig. 3. After cooling to room temperature, the pressure was recovered to 10^{-6} Pa. Following that procedure, the environmental dry gas was introduced into the UHV chamber *via* a variable leak valve. The purity of the environmental dry gas was 99.7% for oxygen and 99.999% for nitrogen. The pressure was controlled using a variable leak valve and measured with a B-A gauge over the range of 10^{-6} to 10^{1} Pa and a Bourdon gauge for −0.1 to +0.11 MPa. The measurement was carried out just after achieving the target pressure, and the environmental gas was kept flowing.

Fig. 4 shows the transfer characteristics in the different environmental gases (a) oxygen and (b) nitrogen. The oxygen environment led to remarkably increased hysteresis due to the gas dosing, while nitrogen resulted in small changes in the hysteresis. We note that the device showed similar I_{ds}–V_g curves (black line) before introducing the environmental gas; furthermore, the maximum I_{ds} at the highest V_g was decreased compared with that observed in the UHV environment in both the oxygen and nitrogen environment cases. The percentage reduction in the on-state current, *i.e.*, the I_{ds} at $V_g = 80$ V, was ∼63% for the 1 atm oxygen environment and ∼20% for 1 atm nitrogen, respectively. Oxygen has an acceptor nature and traps electrons on this surface. We observed interesting behavior in
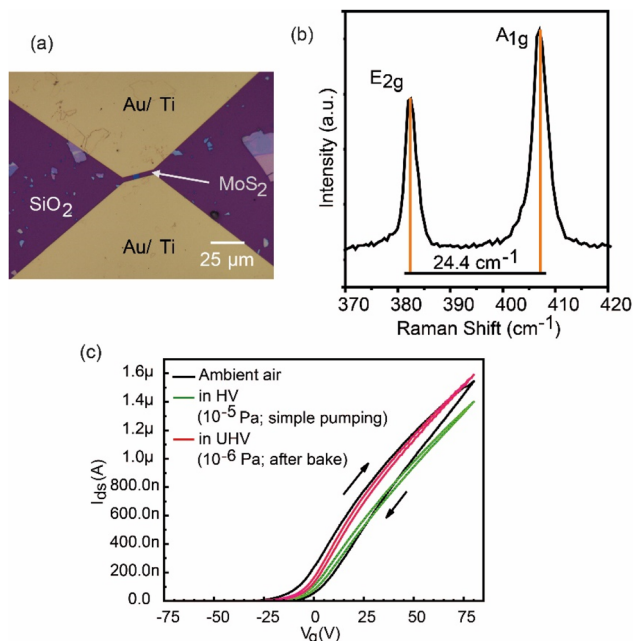
Fig. 2 (a) Optical image of an FFT with a four-layer MoS₂ channel on a SiO₂/Si substrate. (b) Raman spectrum of the MoS₂ flake used in this device. (c) The series of transfer characteristic (I_{ds}–V_g) curves of the MoS₂ transistor. I_{ds}–V_g curves for $V_{ds} = 50$ mV in air (black), high vacuum (green), and ultra-high vacuum (red). The scan rate for the measurement of the I_{ds}–V_g curves was approximately 5.0 V s⁻¹. The sweep directions of V_G are indicated by arrows. All measurements were performed in the dark at room temperature.

the hysteresis in tests of the gas pressure effect and photo-response in an oxygen environment. Sulfur-vacancies, namely, chalcogen vacancies, favor natural n-type doping in MoS₂ and act as trap centers that enhance the hysteretic behavior in MoS₂ and other 2D TMDs.[28] Our results indicate that the oxygen molecule is greatly preferred to adsorb to and interact with

chalcogen vacancies over nitrogen. In principle, these defects should influence the surface adsorption, which in turn can passivate these donors, affecting both the concentration and the mobility of the carriers in the layer. Based on DFT calculations, the S-vacancy acts as a donor state that lies approximately 0.25–0.5 eV below the conduction-band minimum and gives rise to several new energy states in the forbidden gap.[34,35] Since oxygen has a great effect on hysteresis, the effect of the voltage sweep rate was examined at two different oxygen pressures. Fig. 4(c) and (d) depict the effects of different voltage sweep rates (2.5, 5, and 10 V s⁻¹) on hysteresis at two distinct oxygen pressures, 1000 Pa and 20 000 Pa, respectively. In both instances, it is observed that the hysteresis decreases at the fastest sweep speed. This is because MoS₂ FETs typically have lower hysteresis, since it takes less time for the charge trapping and de-trapping processes to take place. This results in steadier transfer characteristics over the voltage sweep range since the device has less time to interact with charge traps.[36] Fig. 4(e) and (f) demonstrate the output characteristics (I_{ds}–V_{ds}) of the device with a pristine surface and after oxygen injection (1.0×10^{-3} Pa), respectively. After oxygen was introduced at a pressure of 1.0×10^{-3} Pa, the device output characteristics showed very slight changes in the hysteresis curves, but the drain current decreased as linearity was lost. This suggests that when the amount of carrier trapping/scattering centers increases slightly, there is a small decrease in electron injection from the Au/Ti contacts into MoS₂. This behavior is similar to the transfer characteristics measured in Fig. 4(a), which shows that no visible changes were observed in the hysteresis curves after the introduction of oxygen at 1.0×10^{-3} Pa. We hypothesized that if the output characteristics were measured at a higher oxygen dose, a clear change in the hysteresis curve would be observed. Linear growth of I_{ds} with V_{ds} indicates good ohmic contact between the electrodes and MoS₂ at the pristine surface.[37] Following the introduction of oxygen, I_{ds} dropped and deviated
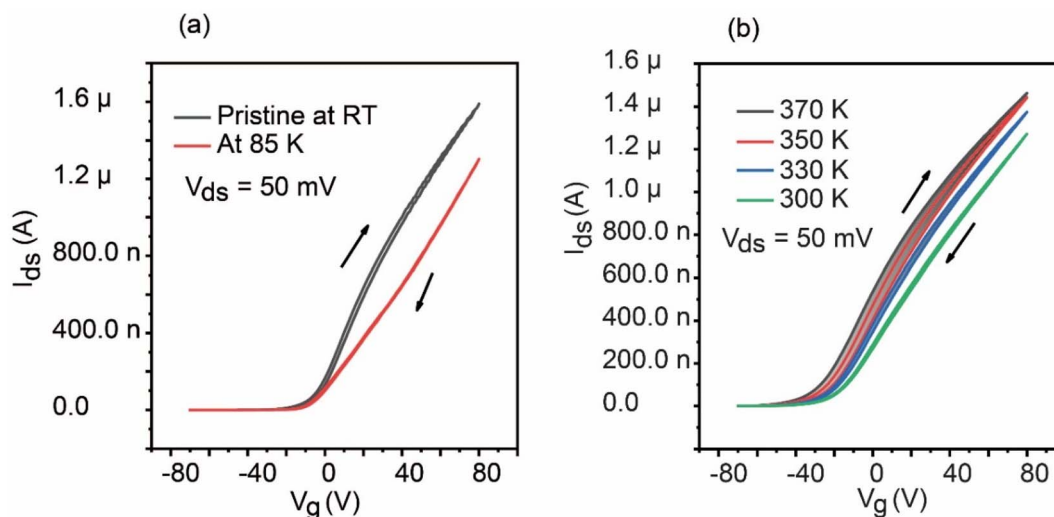

Fig. 3 Series of I_{ds}–V_g curves for $V_{ds} = 50$ mV in dark conditions at various temperatures. (a) RT (black) to 85 K (red) for the cooling experiment. (b) 370 (black) to 300 K (green) after the baking procedure. The V_g sweep started from −70 V and was ramped at a rate of 5 V s⁻¹. The sweep directions of V_g are indicated by the arrows.
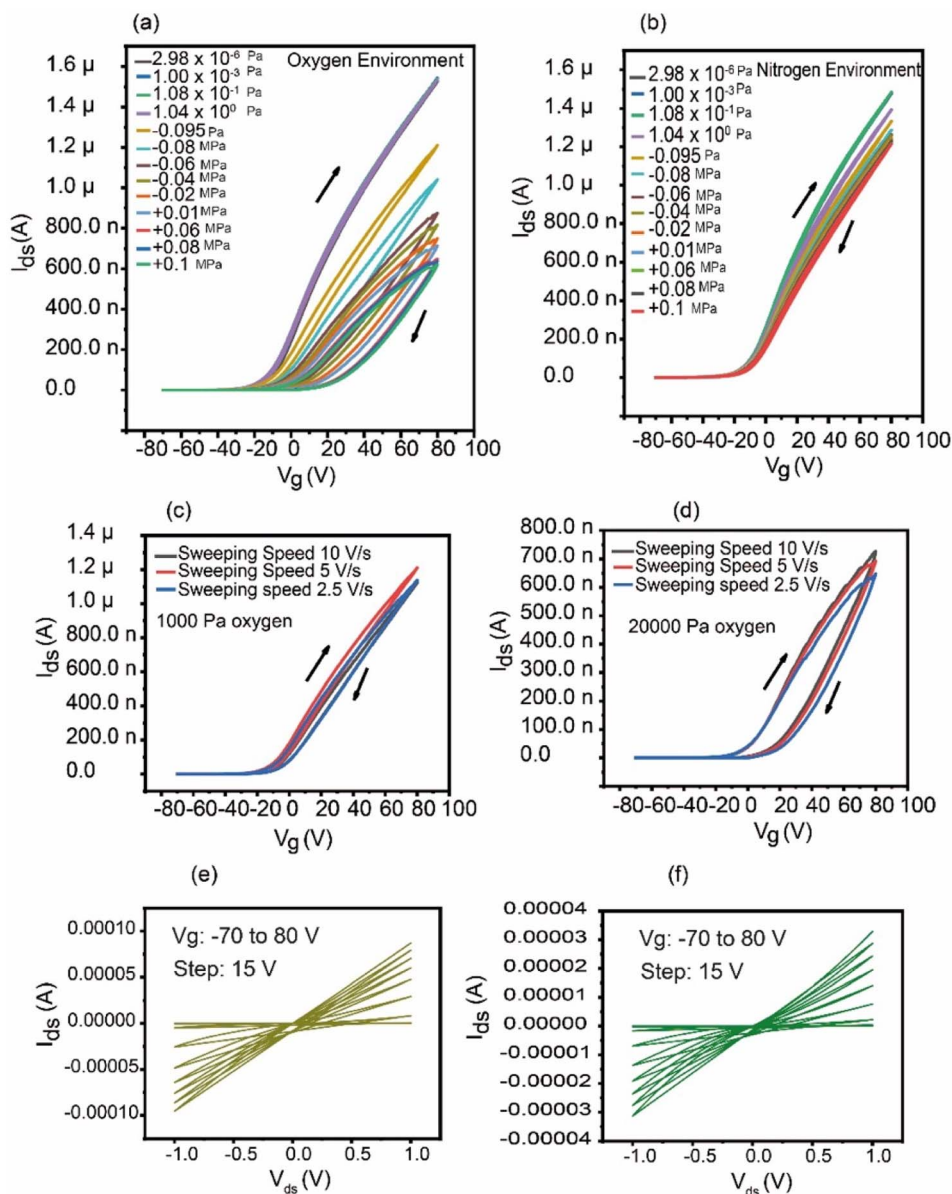
Fig. 4 Environmental effects on the hysteresis curve: (a) oxygen environment. (b) Nitrogen environment. (c) Voltage sweep speed effect at 1000 Pa of oxygen. (d) Voltage sweep speed effect at 20 000 Pa of oxygen. The sweep directions of V_G are indicated by the arrows. (e) Output characteristics of the pristine device. (f) Output characteristics after the introduction of oxygen (1.0×10^{-3} Pa).

from linearity at increasing V_g, particularly in the positive voltage range, which may be because of the adsorption of oxygen at the vacant sites of MoS_2, where it acts as an electron acceptor. The voltage sweep direction was reversed (80 V to −70 V) to investigate whether any changes in the duration of the charge trapping/de-trapping process would occur, as displayed
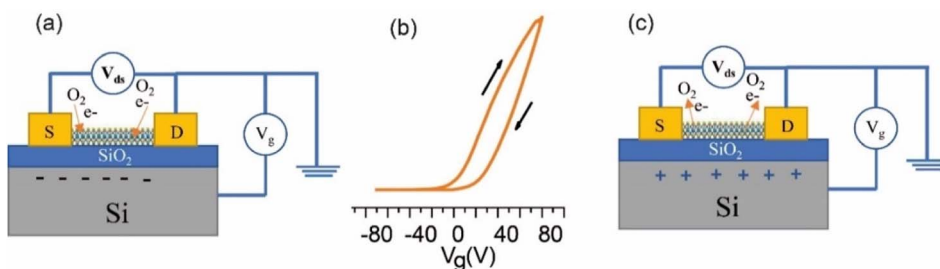

Fig. 5 Illustration of charge transfer between the adsorbed O_2 molecules and MoS_2. (a) $V_g = -80$ V and (c) $V_g = 70$ V in the I_{ds}–V_g plot (b).

in Fig. S4.† However, no significant change was observed. Peize Han *et al.* described the mechanism of the origin of hysteresis induced by oxygen and water molecules under ambient conditions.[38] The mechanism for the origin of hysteresis in the presence of only oxygen is shown in Fig. 5 in a similar manner.

The adsorption of molecules at these vacancy sites passivates the donors, resulting in a reduction in the electron concentration in the conduction band, as shown in Fig. 5(a). Since it is highly electronegative, oxygen has an acceptor nature and traps electrons from MoS_2. When a positive voltage is applied to the gate channel, as shown in Fig. 5(c) to the right of the hysteresis displayed in Fig. 5(b), the MoS_2 surface becomes electron-rich. Electrons fill the charge traps, rendering them neutral and leading to a positive V_{TH} shift. The electrons remain trapped until the reverse sweep, during which they are de-trapped.[39] Oxygen molecules easily adsorb on the surface by accepting electrons from the surface ($O_2 + e^- \rightarrow O_2^-$). Due to the decrease in electron density for molecule adsorption, the on-state current decreases and V_{th} shifts to positive. At a negative gate voltage, the MoS_2 channel becomes filled with holes and the adsorbed molecules return electrons to surface ($O_2^- + h \rightarrow O_2$),[32,40] while molecule desorption happens as shown in Fig. 5(a) to the left.[38] Therefore, at negative gate voltages, the concentration of adsorbed molecules and electron-filled traps (along with their hole-doping effect) is suppressed, and the threshold shifts towards negative gate voltages. Theoretically, DFT calculations

predict that the physisorption of O_2 molecules on MoS_2 occurs with a binding energy of 79 meV, and that approximately 0.04 electrons per O_2 are transferred to the molecules.[41]

To clarify the charge trapping effect due to the environmental gas, we plotted the differential threshold voltage (ΔV_{TH}) *versus* gas pressure as shown in Fig. 6(a). The method of calculation for the threshold voltage is shown in the SI. The differential threshold voltages $\Delta V_{TH} = V_{TH2} - V_{TH1}$ in different sweep directions, where V_{TH1} is for the forward (off–on direction) sweep and V_{TH2} for the backward (on–off) sweep, are defined as the voltages at which the drain–source current is I_{ds} = 1 nA. The ΔV_{TH} value indicates the separation degree of the hysteresis. In both the oxygen and nitrogen gas introduction conditions, V_{TH1} and V_{TH2} were shifted in the positive direction. In an oxygen environment, V_{TH1} shifted much more than V_{TH2}, and as a result, a large hysteresis appeared. The separation of the hysteresis curve increased rapidly from an oxygen partial pressure of about 1000 Pa, and ΔV_{TH} exceeded 36 V at 1 atm. While the hysteresis in the nitrogen environment did not show such a clear difference compared to that observed for oxygen, it did exhibit a slight increase in the hysteresis compared with that observed under UHV, and the difference in the threshold voltage depending on the sweep direction widened to about 3.2 V at 1 atm. The mobility of the device following oxygen input is shown in Fig. 6(b). The device's mobility dropped significantly under these conditions from around 52 to 15 $cm^2\,V^{-1}\,s^{-1}$,
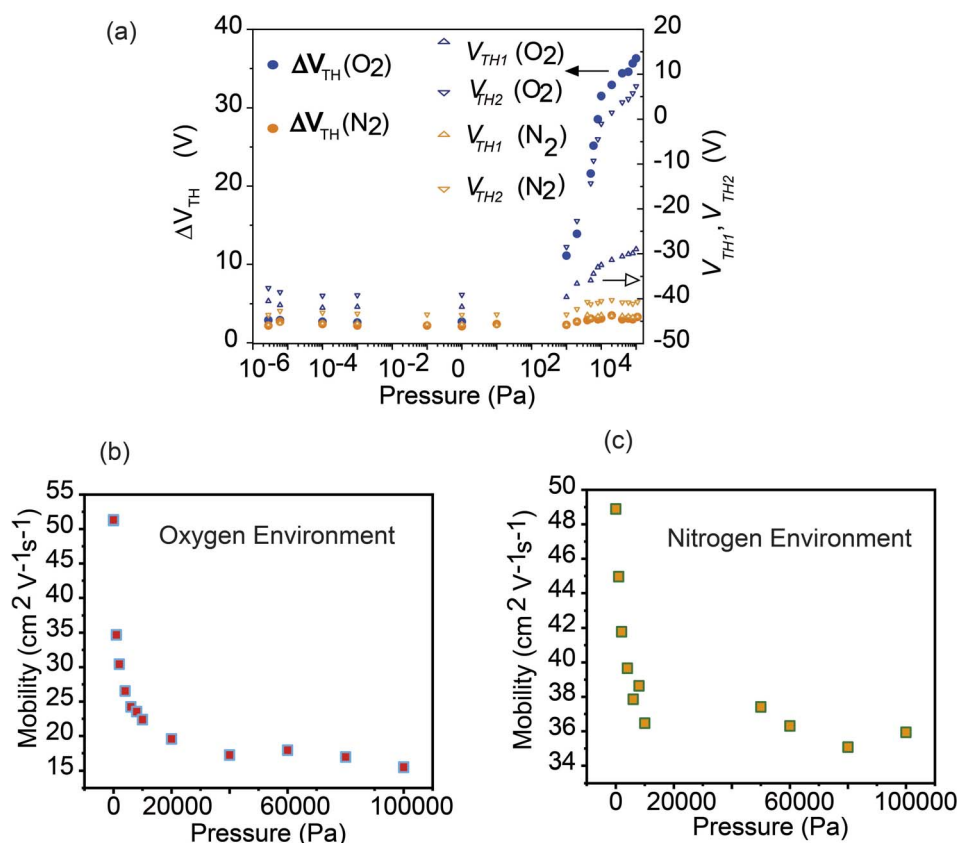

Fig. 6 (a) The threshold gate voltages V_{th1}, V_{th2} (open triangles) and $\Delta V_{th} = V_{th2} - V_{th1}$ (filled circles) as functions of relative gas pressure. (b) Mobility as a function of oxygen pressure. (c) Mobility as a function of nitrogen pressure.
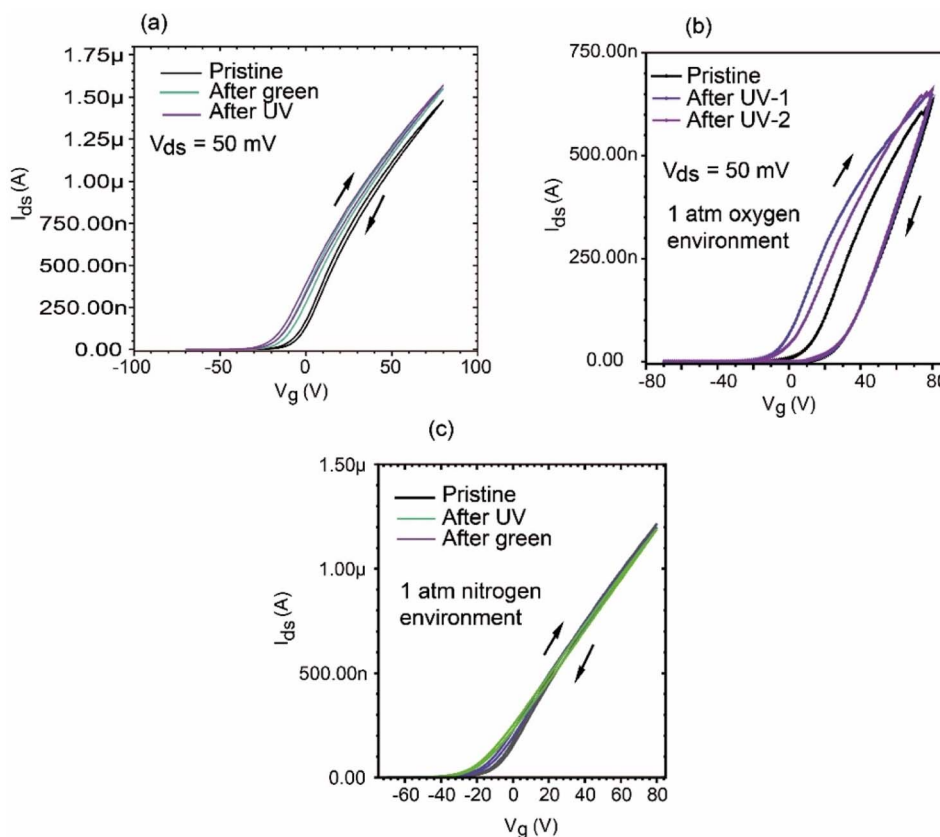
Fig. 7 Series of hysteresis curves indicating the "light illumination effect" for the pristine surface. (a) Under high vacuum (10^{-6} Pa). Pristine (black), after UV light illumination (purple) for 7 s, and after green light illumination (green) for 4 s. (b) In a 1 atm oxygen environment, after UV light illumination for 43 s. (c) In a 1 atm nitrogen environment. V_{ds} was set to 50 mV. The V_g sweeps started from -70 V at 5 V s^{-1}. The sweep directions of V_g are indicated by the arrows.

while in the case of nitrogen, it dropped from approximately 49 to 36 cm^2 V^{-1} s^{-1}, as shown in Fig. 6(c). This phenomenon shows that, in comparison to nitrogen, oxygen has a more significant impact on the device performance, leading to greater hysteresis.

Considering the applications of MoS$_2$-based FETs to optical functions, it is particularly important to investigate the change in the transfer curve due to light irradiation under various environmental (gas) conditions. In general, the photo-response of the MoS$_2$-FET device is determined using the I_d variation under UV and green light irradiation, as shown in Fig. 7(a). The I_d variation is also helpful to understand photo-switching, persistent photoconductivity, and the relaxation of photocurrent, *etc.* In this work, we focused on the changes in the

hysteresis of the I_{ds}–V_G curve due to light irradiation in the vacuum and gas environments. The light irradiation effect on the I_{ds}–V_{ds} curves in oxygen and nitrogen environments is shown in Fig. 7(b) and (c), respectively. The light irradiation was carried out using an LED array mounted inside the chamber. The wavelengths of the LEDs were 365 nm (UV) and 525 nm (visible green). The driving current for the LEDs was $I_f = 26$ mA. The I_{ds}–V_G measurements were performed just after light irradiation in the dark. The on-state current for I_{ds} at $V_G = 80$ V was increased after light irradiation. When the MoS$_2$-FET device in the vacuum and nitrogen environment was irradiated with light, both the threshold voltage V_{TH1} (forward) and V_{TH2} (backward) shifted in the negative direction, and as a result, we obtained almost the same ΔV_{TH}. Interestingly, in the case of the

Table 1 Main factors in the hysteresis of MoS$_2$-FET

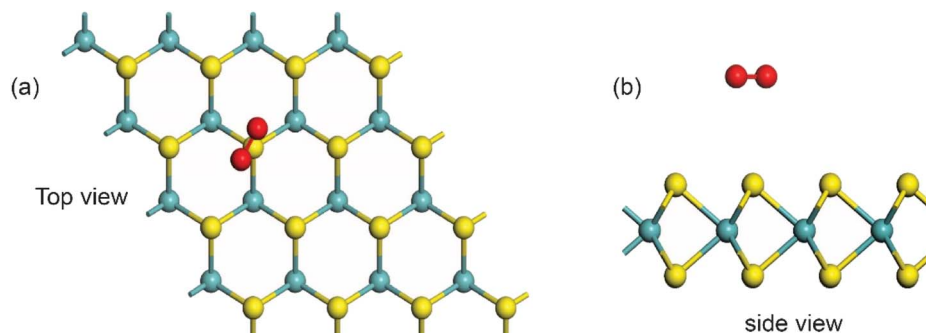| Thickness of SiO$_2$	Number of layers of MoS$_2$	Hysteresis conditions	References
270 nm	Bulk layer	Oxygen, nitrogen, and air and nitrogen with varying relative humidities	27
—	CVD-grown monolayer	Oxygen, nitrogen, hydrogen and methane	28
300 nm	Monolayer	Humidity and illumination	29
300 nm	Monolayer	MoS$_2$ itself	33
285 nm	Monolayer	Water and oxygen	34
300 nm	Four layers	Oxygen, nitrogen, temperature, UV, and green light	Present work

Fig. 8 Optimized model of the interaction between MoS$_2$ and oxygen: (a) top view; (b) side view.

device in an oxygen environment, the light irradiation caused the threshold voltage of V_{TH1} to shift appreciably in the negative direction, while V_{TH2} was pinned to almost the same value, and the on–off (backward) curve kept almost the same shape. The differential threshold ΔV_{TH} became 10 times larger than that before light irradiation. The light irradiation seems to result in modification of the band structure of MoS$_2$, as shown in Fig. 7(a) in the case of UHV. Basically, photo-irradiation activates the trap state intermediate band gap and produces photoconductivity. While the UHV and nitrogen environment results show a similar response to the light irradiation, characteristic features were observed in the oxygen environment. Light substantially increases the channel conductance for photoconductive and photogating effects[9,42] Both temperature and light increase the availability of thermally or photo-generated minority carriers (holes) in MoS$_2$ and enable additional processes of positive charge trapping, which further enhance the hysteresis. During the forward V_G sweep, adsorbed oxygen molecules easily desorb from the surface supported by the light excitation and hole-producing effect, while O$_2$ desorption in the backward V_G sweep might be suppressed due to reduced hole-creation effect. The reason for the trapping on-to-off curve in I_d–V_G after light irradiation in oxygen environment seems to be complicated. Further study is required to identify the origin of the photo-response in detail, *e.g.*, other gas adsorbates on the device channel and/or chemical impurities between the SiO$_2$ interface.

We also investigated the recovery process. In the case of light irradiation in an oxygen or nitrogen environment at 1 atm, the I_{ds} curve returned to almost its original state after the device was left in the dark for several days, with some dependence on the time of light irradiation. In contrast, the effect of light irradiation on MoS$_2$-FET in an ultra-high vacuum seemed to persist for an exceedingly long time. The hysteresis curve did not return to its original state over after 100 h. Again, heating the device under vacuum was effective to nearly recover the device to its pristine state under vacuum.

A comparison table is given in Table 1 regarding the main factors responsible for the device hysteresis. From the table, it is clear that oxygen is the main factor in the hysteresis in the field effect transistor devices, which is consistent with our findings.

To investigate the electron transfer process, the interaction between an MoS$_2$ slab and an oxygen molecule was investigated

via density functional theory (DFT). The optimized model of MoS$_2$ with oxygen is shown in Fig. 8 in (a) top view and (b) side view. All DFT calculations were performed using the Vienna *ab initio* simulation package (VASP)[43] with the generalized gradient approximation (GGA) – Perdew–Burke–Ernzerhof (PBE) functionality. The energy cutoff of the plane-wave basis was set to 400 eV. For energy minimization, the convergence threshold was set at 10^{-5} eV, while for force, it was set at 0.01 eV Å^{-1}. For the structural relaxation, the Brillouin zone was represented using a $3 \times 3 \times 1$ Monkhorst–Pack k-point mesh, and for the self-consistent computations, a $10 \times 10 \times 1$ mesh. To prevent interactions between monolayer MoS$_2$, the $4 \times 4 \times 1$ MoS$_2$ slab in the supercell was vacuum-sealed at a thickness of 15 Å. Grimme's expression implemented the vdW correction for physical adsorption configurations.[44] A significant amount of oxygen is analytically physisorbed onto the MoS$_2$ FET when oxygen is injected into the vacuum chamber. Bader analysis indicates that the physisorbed oxygen molecules are electron donors and cause p-type doping. Our theoretical models closely align with earlier atomic-scale reports.[45] Bader analysis shows that about 1.06 e$^-$ is transferred per molecule from MoS$_2$ to oxygen molecule.

In terms of data reproducibility, two different MoS$_2$-FET devices were used under the same oxygen exposure conditions, as shown in Fig. S5.† It is clearly seen that effect of oxygen on the hysteresis behavior of the two devices is almost the same. We believe that this is possible due to the benefit of using an ultra-high vacuum chamber.

Conclusion

We have described the distinctive hysteresis behavior in the transfer characteristics seen under different circumstances for back-gated field-effect transistors with an exfoliated MoS$_2$ channel. We have discovered that changes in temperature, ambient gas, or light irradiation all significantly increase hysteresis. The hysteresis in a 1 atm oxygen environment exhibits distinctive behavior, which we attribute to the oxygen molecule acting as a charge acceptor on the MoS$_2$ surface. It is possible that oxygen molecules are a better charge acceptor than nitrogen molecules based on the decrease in the device current value when it is in the ON state. We infer that, in addition to oxygen and nitrogen adsorbates on the passivated

device surface, intrinsic defects in MoS_2, such as S vacancies, which lead to effective adsorbate trapping, are crucial in the hysteresis behavior. Both temperature and light increase the amount of thermally or photogenerated minority carriers (holes) in MoS_2. This causes further positive charge trapping processes, which amplify the hysteresis.

Data availability

Any kind of data will be supplied if requested.

Author contributions

Muhammad Shamim Al Mamun: writing – original draft, visualization, methodology, investigation, conceptualization. Yasuyuki Sainoo: writing – original draft, visualization, methodology, investigation, conceptualization. Tsuyoshi Takaoka: writing – review & editing, investigation. Atsushi Ando: writing – review & editing. Tadahiro Komeda: writing – review & editing, project administration, funding acquisition.

Conflicts of interest

There are no conflicts to declare.

Acknowledgements

References

1 Z. Lin, A. McCreary, N. Briggs, S. Subramanian, K. Zhang, Y. Sun, X. Li, N. J. Borys, H. Yuan, S. K. Fullerton-Shirey, A. Chernikov, H. Zhao, S. McDonnell, A. M. Lindenberg, K. Xiao, B. J. LeRoy, M. Drndić, J. C. M. Hwang, J. Park, M. Chhowalla, R. E. Schaak, A. Javey, M. C. Hersam, J. Robinson and M. Terrones, *2D Materials*, 2016, **3**, 042001.
2 A. Di Bartolomeo, *Phys. Rep.*, 2016, **606**, 1–58.
3 N. T. Trung, M. I. Hossain, M. I. Alam, A. Ando, O. Kitakami, N. Kikuchi, T. Takaoka, Y. Sainoo, R. Arafune and T. Komeda, *ACS Omega*, 2020, **5**, 28108–28115.
4 M. S. A. Mamun, H. Waizumi, T. Takaoka, M. I. Alam, Y. Tanaka, A. Ando, Z. Wang and T. Komeda, *Nanotechnology*, 2021, **32**, 075501.
5 H. Waizumi, M. Shamim Al Mamun, T. Takaoka, M. Iftekharul Alam, Y. Tanaka, A. Ando, Z. Wang, R. Arafune and T. Komeda, *Appl. Surf. Sci.*, 2022, **571**, 151252.
6 X. Li and H. Zhu, *J. Materiomics*, 2015, **1**, 33–44.
7 J. K. Ellis, M. J. Lucero and G. E. Scuseria, *Appl. Phys. Lett.*, 2011, **99**, 261908.
8 K. F. Mak, C. Lee, J. Hone, J. Shan and T. F. Heinz, *Phys. Rev. Lett.*, 2010, **105**, 136805.
9 A. Di Bartolomeo, L. Genovese, T. Foller, F. Giubileo, G. Luongo, L. Croin, S. J. Liang, L. K. Ang and M. Schleberger, *Nanotechnology*, 2017, **28**, 214002.
10 A. Di Bartolomeo, A. Pelella, X. Liu, F. Miao, M. Passacantando, F. Giubileo, A. Grillo, L. Iemmo, F. Urban and S.-J. Liang, *Adv. Funct. Mater.*, 2019, **29**, 1902483.
11 M.-L. Tsai, S.-H. Su, J.-K. Chang, D.-S. Tsai, C.-H. Chen, C.-I. Wu, L.-J. Li, L.-J. Chen and J.-H. He, *ACS Nano*, 2014, **8**, 8317–8322.
12 W. Zhang, J.-K. Huang, C.-H. Chen, Y.-H. Chang, Y.-J. Cheng and L.-J. Li, *Adv. Mater.*, 2013, **25**, 3456–3461.
13 J. H. Sim, S. C. Song, P. D. Kirsch, C. D. Young, R. Choi, D. L. Kwong, B. H. Lee and G. Bersuker, *Microelectron. Eng.*, 2005, **80**, 218–221.
14 M. S. A. Mamun, Y. Sainoo, T. Takaoka, H. Waizumi, Z. Wang, M. I. Alam, A. Ando, R. Arafune and T. Komeda, *Phys. Chem. Chem. Phys.*, 2021, **23**, 27273–27281.
15 M. S. Al Mamun, H. Waizumi, T. Takaoka, Z. Wang, A. Ando and T. Komeda, *Org. Electron.*, 2024, **126**, 106989.
16 M. S. A. Mamun, Y. Tanaka, H. Waizumi, T. Takaoka, Z. Wang, M. I. Alam, A. Ando, M. Fukuyama, A. Hibara and T. Komeda, *Phys. Chem. Chem. Phys.*, 2020, **22**, 27724–27731.
17 K. S. Novoselov, D. Jiang, F. Schedin, T. J. Booth, V. V. Khotkevich, S. V. Morozov and A. K. Geim, *Proc. Natl. Acad. Sci. U. S. A.*, 2005, **102**, 10451–10453.
18 K. S. Novoselov, A. K. Geim, S. V. Morozov, D. Jiang, M. I. Katsnelson, I. V. Grigorieva, S. V. Dubonos and A. A. Firsov, *Nature*, 2005, **438**, 197–200.
19 K. S. Novoselov, A. K. Geim, S. V. Morozov, D. Jiang, Y. Zhang, S. V. Dubonos, I. V. Grigorieva and A. A. Firsov, *Science*, 2004, **306**, 666–669.
20 Y. Y. Wang, R. X. Gao, Z. H. Ni, H. He, S. P. Guo, H. P. Yang, C. X. Cong and T. Yu, *Nanotechnology*, 2012, **23**, 495713.
21 H. Li, Q. Zhang, C. C. R. Yap, B. K. Tay, T. H. T. Edwin, A. Olivier and D. Baillargeat, *Adv. Funct. Mater.*, 2012, **22**, 1385–1390.
22 M. Tosun, D. Fu, S. B. Desai, C. Ko, J. Seuk Kang, D.-H. Lien, M. Najmzadeh, S. Tongay, J. Wu and A. Javey, *Sci. Rep.*, 2015, **5**, 10990.
23 M. Egginger, S. Bauer, R. Schwödiauer, H. Neugebauer and N. S. Sariciftci, *Monatsh. Chem.*, 2009, **140**, 735–750.
24 H. Li, Z. Yin, Q. He, H. Li, X. Huang, G. Lu, D. W. H. Fam, A. I. Y. Tok, Q. Zhang and H. Zhang, *Small*, 2012, **8**, 63–67.
25 M. Fontana, T. Deppe, A. K. Boyd, M. Rinzan, A. Y. Liu, M. Paranjape and P. Barbara, *Sci. Rep.*, 2013, **3**, 1634.
26 M. Gobbi, S. Bonacchi, J. X. Lian, A. Vercouter, S. Bertolazzi, B. Zyska, M. Timpel, R. Tatti, Y. Olivier, S. Hecht, M. V. Nardi, D. Beljonne, E. Orgiu and P. Samorì, *Nat. Commun.*, 2018, **9**, 2661.
27 Y. Shimazu, M. Tashiro, S. Sonobe and M. Takahashi, *Sci. Rep.*, 2016, **6**, 30084.
28 F. Urban, F. Giubileo, A. Grillo, L. Iemmo, G. Luongo, M. Passacantando, T. Foller, L. Madauß, E. Pollmann, M. P. Geller, D. Oing, M. Schleberger and A. Di Bartolomeo, *2D Materials*, 2019, **6**, 045049.
29 D. J. Late, B. Liu, H. S. S. R. Matte, V. P. Dravid and C. N. R. Rao, *ACS Nano*, 2012, **6**, 5635–5641.
30 H. Qiu, L. Pan, Z. Yao, J. Li, Y. Shi and X. Wang, *Appl. Phys. Lett.*, 2012, **100**, 123104.

31 T. Li, G. Du, B. Zhang and Z. Zeng, *Appl. Phys. Lett.*, 2014, **105**, 093107.

32 K. Cho, W. Park, J. Park, H. Jeong, J. Jang, T.-Y. Kim, W.-K. Hong, S. Hong and T. Lee, *ACS Nano*, 2013, **7**, 7751–7758.

33 J. Shu, G. Wu, Y. Guo, B. Liu, X. Wei and Q. Chen, *Nanoscale*, 2016, **8**, 3049–3056.

34 A. Di Bartolomeo, L. Genovese, F. Giubileo, L. Iemmo, G. Luongo, T. Foller and M. Schleberger, *2D Materials*, 2018, **5**, 015014.

35 S. Deb, P. Bhattacharyya, P. Chakrabarti, H. Chakraborti, K. Das Gupta, A. Shukla and S. Dhar, *Phys. Rev. Appl.*, 2020, **14**, 034030.

36 C. Li, C. Wen, R. Zeng, S. Zeng, Z. J. Qiu, Z. Zhang, S. L. Zhang and D. Wu, *IEEE Electron Device Lett.*, 2020, **41**, 1356–1359.

37 J. Shan, J. Li, X. Chu, M. Xu, F. Jin, X. Wang, L. Ma, X. Fang, Z. Wei and X. Wang, *RSC Adv.*, 2018, **8**, 7942–7948.

38 P. Han, E. R. Adler, Y. Liu, L. St Marie, A. El Fatimy, S. Melis, E. Van Keuren and P. Barbara, *Nanotechnology*, 2019, **30**, 284004.

39 I. M. Datye, A. J. Gabourie, C. D. English, K. K. H. Smithe, C. J. McClellan, N. C. Wang and E. Pop, *2D Materials*, 2019, **6**, 011004.

40 J. Pak, M. Min, K. Cho, D.-H. Lien, G. H. Ahn, J. Jang, D. Yoo, S. Chung, A. Javey and T. Lee, *Appl. Phys. Lett.*, 2016, **109**, 183502.

41 S. Tongay, J. Zhou, C. Ataca, J. Liu, J. S. Kang, T. S. Matthews, L. You, J. Li, J. C. Grossman and J. Wu, *Nano Lett.*, 2013, **13**, 2831–2836.

42 M. K. Ghimire, H. Ji, H. Z. Gul, H. Yi, J. Jiang and S. C. Lim, *ACS Appl. Mater. Interfaces*, 2019, **11**, 10068–10073.

43 J. Hafner, *J. Comput. Chem.*, 2008, **29**, 2044–2078.

44 S. Grimme, J. Antony, S. Ehrlich and H. Krieg, *J. Chem. Phys.*, 2010, **132**, 154104.

45 G. Sun, F. Li, T. Wu, L. Cong, L. Sun, G. Yang, H. Xie, A. Mauger, C. M. Julien and J. Liu, *Inorg. Chem.*, 2019, **58**, 2169–2176.